


 Cite this: *Lab Chip*, 2015, 15, 4451

Microfluidic cell-phoresis enabling high-throughput analysis of red blood cell deformability and biophysical screening of antimalarial drugs†

 Aline T. Santoso,^a Xiaoyan Deng,^a Jeong-Hyun Lee,^a Kerryn Matthews,^a Simon P. Duffy,^a Emel Islamzada,^a Sarah M. McFaul,^a Marie-Eve Myrand-Lapierre^a and Hongshen Ma^{*abc}

Changes in red blood cell (RBC) deformability are associated with the pathology of many diseases and could potentially be used to evaluate disease status and treatment efficacy. We developed a simple, sensitive, and multiplexed RBC deformability assay based on the spatial dispersion of single cells in structured microchannels. This mechanism is analogous to gel electrophoresis, but instead of transporting molecules through nano-structured material to measure their length, RBCs are transported through micro-structured material to measure their deformability. After transport, the spatial distribution of cells provides a readout similar to intensity bands in gel electrophoresis, enabling simultaneous measurement on multiple samples. We used this approach to study the biophysical signatures of falciparum malaria, for which we demonstrate label-free and calibration-free detection of ring-stage infection, as well as *in vitro* assessment of antimalarial drug efficacy. We show that clinical antimalarial drugs universally reduce the deformability of RBCs infected by *Plasmodium falciparum* and that recently discovered PfATP4 inhibitors, known to induce host-mediated parasite clearance, display a distinct biophysical signature. Our process captures key advantages from gel electrophoresis, including image-based readout and multiplexing, to provide a functional screen for new antimalarials and adjunctive agents.

 Received 7th August 2015,
Accepted 7th October 2015

DOI: 10.1039/c5lc00945f

www.rsc.org/loc

Introduction

Gel electrophoresis is a fundamental enabling technology for modern molecular biology and genetics that involves transporting molecules, usually DNA or protein, through a nano-structured material (*e.g.* agarose or polyacrylamide gel) using an electric field. The transport speed depends on molecular mass and charge density, which allows the distance covered by each molecular species to indicate their length relative to known controls.¹ We developed an analogous process for red blood cells (RBCs), here termed microfluidic cell-phoresis, where individual cells are transported through a micro-structured material using pressure-driven flow. RBCs undergo repeated deformations in order to slow their progress, such that the distance covered by each cell over a set period of time is indicative of its mechanical deformability (Fig. 1). The

spatial distribution of RBCs after transport is reminiscent of intensity bands formed by DNA molecules in gel electrophoresis, enabling simultaneous measurements on multiple samples.

Changes in RBC deformability has been associated with the pathology of many diseases including malaria,^{2–5} hemoglobinopathies,^{2,6,7} and micronutrient deficiencies.^{8–10} In the case for malaria,⁵ the infected RBCs (iRBCs) develop notable morphological changes from ring, to trophozoite, and to schizont stages, during which time iRBCs become progressively less deformable as the parasites mature and divide. RBC deformability therefore provides a potential physical biomarker for evaluating the status of malaria infection and the efficacy of potential drugs.

The use of RBC deformability in biological assays is currently limited by two key challenges. First, pathological cells typically comprise of only a small fraction of the overall cell sample, and therefore a large number of single cells must be sampled in order to obtain useful data. Second, cell deformability is a non-specific physical parameter, which, like gel electrophoresis, requires parallel experiments using multiple positive and negative controls in order to assay specific biological properties. Traditional bulk-flow methods,

^a Department of Mechanical Engineering, University of British Columbia, 2054-6250 Applied Science Lane, Vancouver, BC, V6T 1Z4 Canada.

E-mail: hongma@mech.ubc.ca

^b Department of Urologic Science, University of British Columbia, Vancouver, BC, Canada

^c Vancouver Prostate Centre, Vancouver General Hospital, Vancouver, BC, Canada

† Electronic supplementary information (ESI) available. See DOI: 10.1039/c5lc00945f

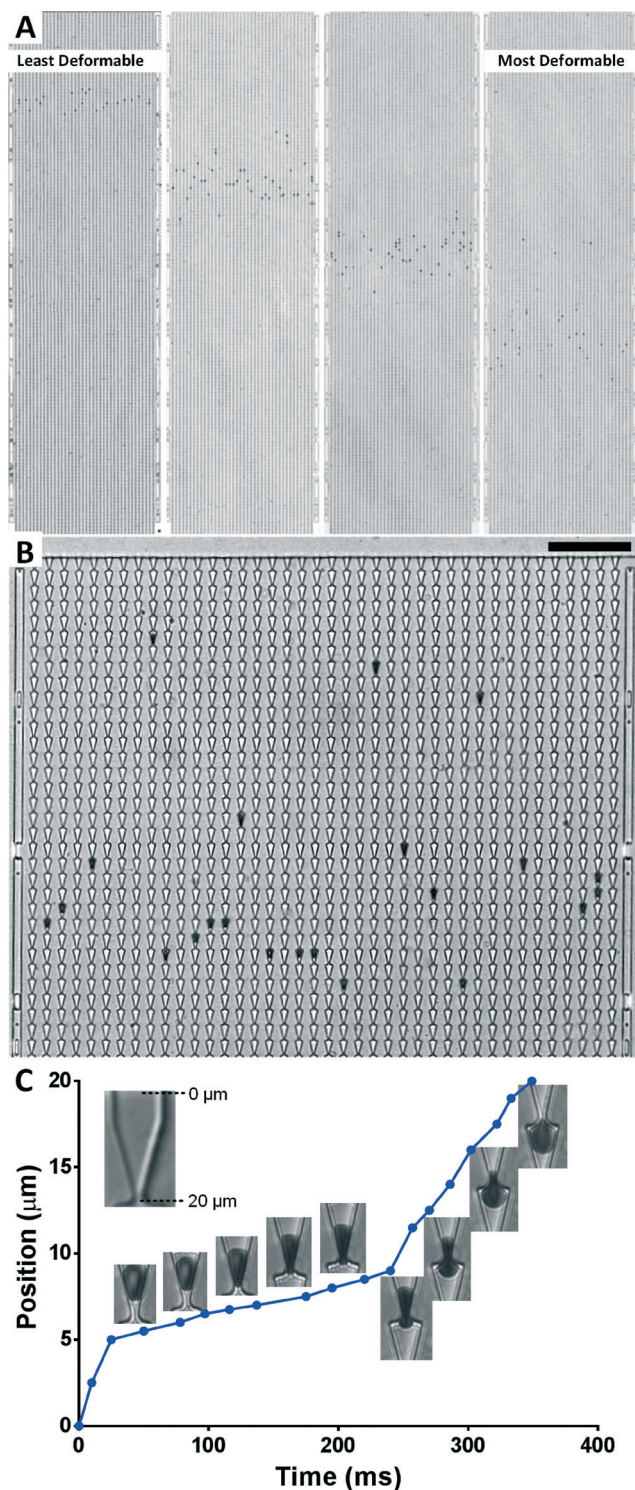


Fig. 1 Microfluidic cell-phoresis. (A) The position of the cells along the device is indicative of their transit speed and hence, their deformability. More deformable cells will travel further along the device than less deformable cells. (B) Micrograph of a zoomed-in section of the deformation microchannels (scale bar = 75 μm). (C) When a constant pressure is applied, the position of the cell along the funnel (inset) shows that the cell acts as a temporary seal against the constriction as it being deformed.

including ektacytometry^{11–14} and micropore filtration,^{15,16} provide a measure of the average deformability of a cell

sample, but obscure information on diseased subpopulations. Single cell methods, such as micropipette aspiration,^{17–19} the atomic force microscope,^{20,21} and optical tweezers,^{22–24} can be used to target pathological cells, but have extremely low throughput because they involve difficult experiments performed by highly skilled technicians. Recent microfluidic methods, based on the measurement of capillary obstruction,^{25,26} as well as transit time^{4,27–29} or transit pressure^{30–32} through micro-scale constrictions, provide greater throughput, but are difficult to parallelize because of the need to monitor the deformation process using a video recording or to integrate electrical sensors on a disposable microfluidic chip. Physical separation process has the potential to separate RBCs based on deformability, but provides less measurement precision.^{33,34} None of these existing approaches have shown the ability to perform simultaneous measurements of multiple samples.

Here, we describe a cell deformation mechanism that captures two key advantages of gel electrophoresis to enable high-throughput, multiplexed cell deformability assays. First, similar to the transport of molecules in nanostructured gels, each cell is deformed through hundreds of micro-scale constrictions in order to average over variations in constriction geometry. Second, the cells are fixed in place after the transport process, which allow them to be analyzed later using automated image analysis, similar to measuring the position of clusters of DNA molecules using a gel imager. This simplified readout enables high-throughput and massively parallelized analysis since a video recording of the transport process is not required. Leveraging these key capabilities, we show that microfluidic cell-phoresis of RBCs enables calibration-free biophysical detection of malaria infection, as well as a functional *in vitro* assay for antimalarial drug efficacy.

Results

Mechanism and design

At the single cell level, microfluidic cell-phoresis involves infusing a cell into a deformation microchannel containing a series of constrictions and deforming this cell through the constrictions using precisely controlled pressure. The constrictions are shaped like a 2D funnel with a minimum opening (1.5–2 μm) significantly smaller than the diameter of RBCs in order to induce significant deformation. The thickness of the microchannel (~4 μm) is designed to constrain the RBCs in a planar orientation and prevents them from re-orienting by rotation. Previously, we showed that a single RBC deformed in this manner forms a temporary seal with the constriction, causing the pressure difference applied across the length of the microchannel to be focused across that cell, thereby enabling remote application of precisely controlled deformation pressure.³¹ Here, this process is applied repeatedly by deforming each cell through hundreds of constrictions in a few minutes in order to average over small variations in the constriction geometry, as well as non-

specific surface interactions between the RBCs and the microstructure.

To increase measurement throughput, the deformation microchannels, each containing hundreds of constrictions, are parallelized. Surrounding the parallel deformation microchannels is a rectangular detour comprised of the loading microchannels, which infuse cells into the deformation microchannels. The detour also comprises bypass microchannels, which provide a dominant hydrodynamic resistance to set the pressure across the deformation microchannels (Fig. 2A and B). Two factors limit the number of deformation microchannels that could be parallelized. First,

the pressure applied across each deformation microchannel (P_D) varies with spatial position because of the pressure drop associated with fluid flow along the loading microchannel. This issue is addressed using a symmetrical fluid circuit to automatically compensate for pressure drops along the loading microchannel (Fig. 2C). Second, the pressure applied across one deformation microchannel depends on whether other deformation microchannels are occupied with cells. The bypass microchannel (Fig. 2A) dictates the pressure across the deformation microchannels, but a fraction of this pressure is dropped across the loading microchannel. Specifically, the fluid streamlines in the occupied deformation

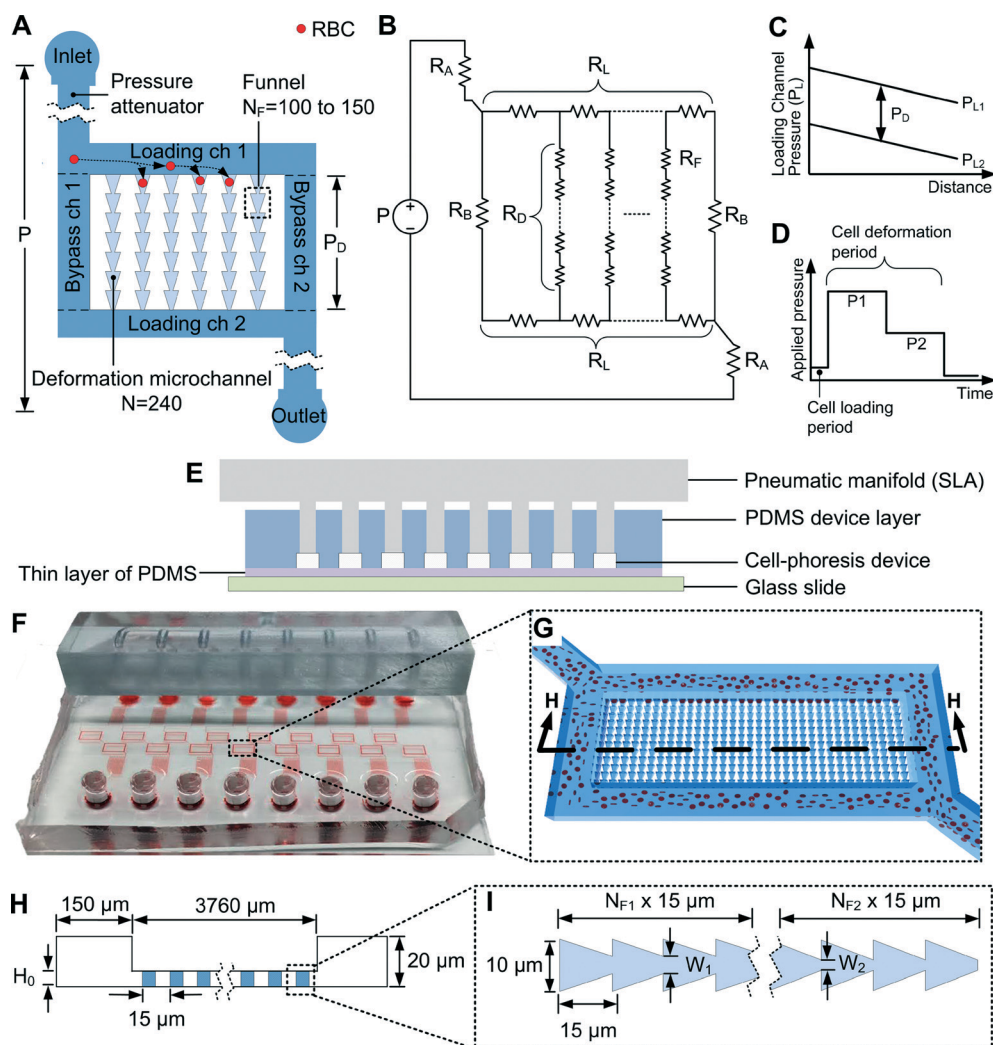


Fig. 2 Design of the microfluidic cell-phoresis mechanism. (A) Structure and components of a single microfluidic cell-phoresis array. N_F and N are the number of funnels in series and the number of deformation microchannels in parallel. P and P_D are the externally applied pressure and the deformation pressure, which is attenuated by the attenuation factor, α . (B) Equivalent hydrodynamic circuit for the microfluidic cell-phoresis array, where R_A , R_B , R_L , R_D and R_F are the hydrodynamic resistances of the attenuator microchannels, bypass microchannels, loading microchannels, deformation microchannel, and individual funnel constrictions. (C) Pressure in the two loading microchannels (P_L) as a function of distance. (D) Pressure waveform applied across the deformation microchannel. (E) Cross-section of the cell-phoresis chip together with the pneumatic manifold to show the overall structure. (F) The microfluidic cell-phoresis chip with 8 parallel arrays. (G) 3D model of a single microfluidic cell-phoresis array. (H) Cross-section of the device showing the detailed geometry (ESI S4†) of bypass and deformation microchannels. H_0 is the thickness of the deformation microchannels. (I) Detailed design of a deformation microchannel containing two sizes of funnel constrictions. W_1 and W_2 are the funnel pore sizes. N_{F1} and N_{F2} are the numbers of funnels in each series.

microchannels are blocked and skewed to feed the unoccupied microchannels, resulting in a different deformation pressure across occupied and unoccupied deformation microchannels (P_D). Here, we call this inconsistency the multiplexing error (E_M) (ESI S1†). We overcame this limitation by ensuring that the hydrodynamic resistance of the deformation microchannels (R_D), is much greater than the hydrodynamic resistance of the loading microchannels (R_L , Fig. 2B), to achieve constant pressure drop in each deformation microchannel (Fig. 2C).

To generate the minute and precisely controlled pressures required to deform individual RBCs (P_D), a pressure attenuator fluidic circuit consisting of a branched microchannel network is attached across a small segment of a long microchannel.³⁵ This microchannel network attenuates an externally applied pressure (P) by a factor equal to the resistance ratio (α) of the bypass microchannels (R_B) and the long inlet microchannel (R_A) to generate the deformation pressure (P_D).

The process for microfluidic cell-phoresis begins by infusing single RBCs into the mouth of the deformation microchannels *via* the loading microchannel at a pressure that is insufficient for them to transit (ESI S2A†). Once the majorities of the deformation microchannels are filled with RBCs, a sequence of deformation pressures are applied to transit the cells through the constrictions (Fig. 2D) (ESI S2B†). After the deformation process, the applied pressure is shut off and the final position of each cell in the deformation microchannel is fixed in position, similar to DNA bands after gel-electrophoresis. This final position of the cells in the deformation microchannel is analyzed using semi-automated imaging software and is used to infer cell deformability (ESI S3†). Since the microfluidic cell-phoresis mechanism does not require video recording of the process, multiple experiments can be performed simultaneously. Our prototype device (Fig. 2E–F) consists of 8 independent microfluidic cell-phoresis arrays (Fig. 2F–I) pressurized simultaneously using a pneumatic manifold (manufactured using stereolithography by Fineline Prototyping, MN, USA).

Together, these design elements provide a simple method to deform single RBCs through a series of constrictions using constant pressure. Analogous to gel electrophoresis, where molecules are transported through nanoscale structures, RBCs are transported through microscale structures to allow their inherent deformability to slow their progress. The final position of the RBCs provides a simple readout of the result, enabling automated and massively parallelized assays.

Mechanism validation

To first establish that repeated deformation of RBCs through micro-scale constrictions is an elastic and memory-less process, we measured the position of single cells as a function of time for different applied pressures. The position *versus* time data is highly linear ($r^2 \geq 0.94$), which demonstrate that the deformation process does not irreversibly change the

deformability of RBCs, and that random errors associated with geometrical variability and surface friction does not significantly affect the final position of the cell (Fig. 3A).

To experimentally validate the ability of the microfluidic cell-phoresis mechanism to minimize the aforementioned multiplexing error, we measured the final positions of fresh RBCs from nearly empty ($\leq 10\%$ funnels occupied) and nearly full ($\geq 70\%$ funnels occupied) funnel arrays. The distributions of the threshold pressures from these two cases are statistically identical ($p = 0.57$, Fig. 3B), which confirms that the multiplexing error is less than the natural variability of RBCs.

The sensitivity of the microfluidic cell-phoresis mechanism to differences in RBC deformability was established by measuring the deformability profiles of RBC samples treated with small amounts of glutaraldehyde (GTA). GTA is a common fixative agent, which induces cross-linking and stabilization of proteins in the red blood cell membrane and thus artificially reduces their deformability in a concentration dependent manner.^{36,37} Hence, the sensitivity of the microfluidic cell-phoresis mechanism was validated using GTA treatment ranging from 0.0005% (5 ppm) to 0.002% (20 ppm). Each data set is normalized to a control by dividing the cell's position by the mean position of the control (ESI S5†). The RBC deformability results obtained (Fig. 3C) can reliably distinguish between control and 0.0005% (5 ppm) GTA-treated RBCs ($p < 0.0001$), which is similar to or better than other methods.^{13,28,35,38–40}

To optimize the sensitivity of the mechanism to distinguish minor differences between RBC deformability, we tested 0% and 0.0005% (5 ppm) GTA-treated RBCs (smallest GTA concentration detectable in literature^{13,28,35}) at different applied deformation pressures. Sensitivity improves exponentially ($R^2 = 0.97$) as the deformation pressure decreases (Fig. 3D). This result arises from the relaxation of the RBC membrane after deformation, which typically has a time constant of 0.09–0.25 s.^{18,19,23,26,40,41} At greater applied pressure, RBCs maintain a 'bullet' shape after deformation and do not have the time to relax back to a biconcave disc, and thereby limiting the required amount of deformation in subsequent constrictions (ESI S6†). To minimize experiment time while still maintaining a high sensitivity, an applied pressure waveform of 15 Pa was selected for further experiments.

Using RBC deformability profiling to detect malaria infection

Loss of RBC deformability after infection by *P. falciparum* is well established. Both parasite-derived factors (proteases, phospholipases, lipids),⁴² secreted parasite proteins (RESA, MESA, KAHRP and PfEMP1),^{43–46} the accumulation hemozoin biocrystals in the parasite food vacuole⁴⁷ and oxidative stress experienced by the host RBC⁴⁸ collectively contribute to rigidification of the cell. The impact of these factors may appear paradoxical because, while the rigidification of the host cell may promote its retention in interendothelial cleft of the spleen,⁴⁹ the enhanced rigidification and cytoadherence of iRBCs contribute to their accumulation within the

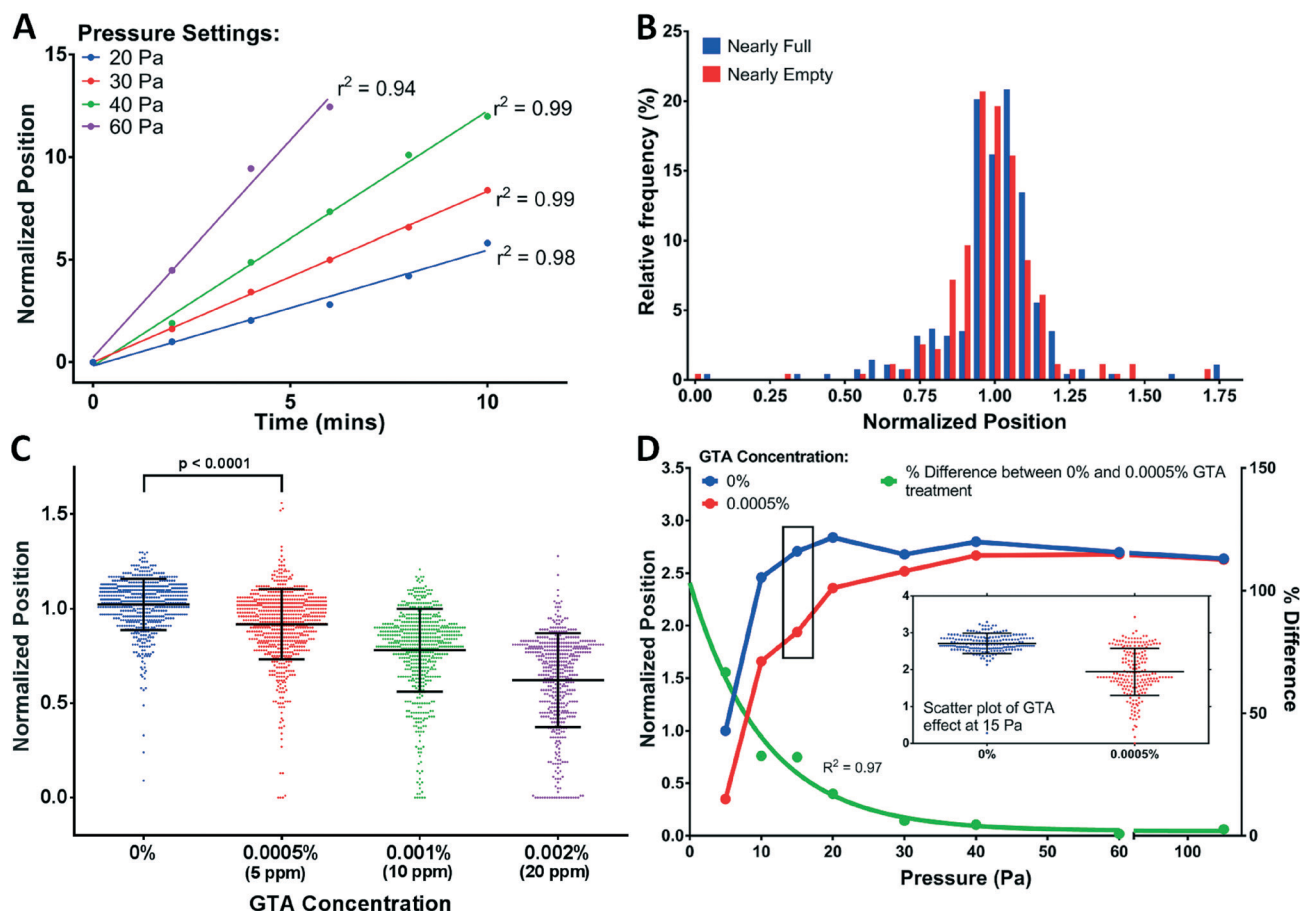


Fig. 3 Validation of the microfluidic cell-phoresis mechanism. (A) Constant speed is observed in 4 test parameters, which indicates that RBC deformations are an elastic and memory-less process ($r^2 \geq 0.94$, $n \geq 125$). (B) Distribution of measured position with the deformation micro-channel array nearly empty ($<10\%$ occupancy, $n = 281$) and nearly full ($>70\%$ occupancy, $n = 583$), which show no distinction ($p = 0.57$). (C) Sensitivity of the microfluidic cell-phoresis mechanism is evaluated using GTA-treated RBCs, showing that this mechanism is able to detect 0.0005% (5 ppm) GTA-treated samples ($p < 0.0001$, $n \geq 509$). (D) The applied pressure waveform is optimized by measuring the % difference between the mean of 0% and 0.0005% (5 ppm) GTA-treated samples to maximize the sensitivity of the microfluidic cell-phoresis mechanism ($n \geq 102$).

microvasculature of the organs, where they evade splenic clearance and contribute to microvascular obstruction.^{50,51} However, the sequestration of iRBCs is typically restricted to more mature stages of iRBC infection (mature trophozoites and schizonts).⁵² Ring stage iRBCs do not express external antigens and may be more likely to be retained in the spleen, upon rigidification, rather than to cytoadhere within organ microvasculature.

While mature stage iRBCs are frequent within an unsynchronized culture we examine whether both unsynchronized iRBCs and the more flexible ring-stage iRBCs could be reliably discriminated from uninfected RBCs based on cellular deformability. We tested unsynchronized iRBC samples at $<5\%$ parasitemia. Expectedly, reduced mean transport distance is directly correlated with greater parasitemia (ESI S7A†). To highlight differences associated with the less deformable iRBCs, we then plotted the cumulative distribution starting from the least deformable cells (Fig. 4A).⁵³ Here, each dataset is normalized to its mean to control for variability in the deformability of uninfected

RBCs. The resulting cumulative distribution curves are ordered according to parasitemia, which indicate the possibility to use these profiles to detect infection down to 0.2% parasitemia. This capability is confirmed by plotting the least deformable 2% of tested cells ($p < 0.0001$, $n \geq 500$, Fig. 4B). Since ring-stage iRBCs are the most interesting stage in the malaria life-cycle for diagnostic purposes, we repeated these experiments on ring-stage synchronized iRBC samples where the cumulative deformability profile is capable of detecting infection down to 1% parasitemia (ESI S7B,† Fig. 4C). Additionally, the number of cells that could not transit past the first funnel constriction is strongly correlated to parasitemia for both unsynchronized ($r^2 = 0.92$, Fig. 4D) and synchronized ring-stage samples ($r^2 = 0.95$, Fig. 4D).

A biophysical assay for antimalarial drug efficacy

We used microfluidic cell-phoresis to study how exposure to antimalarials affects iRBC deformability. Previous studies found that exposure to either chloroquine or artemisinin-

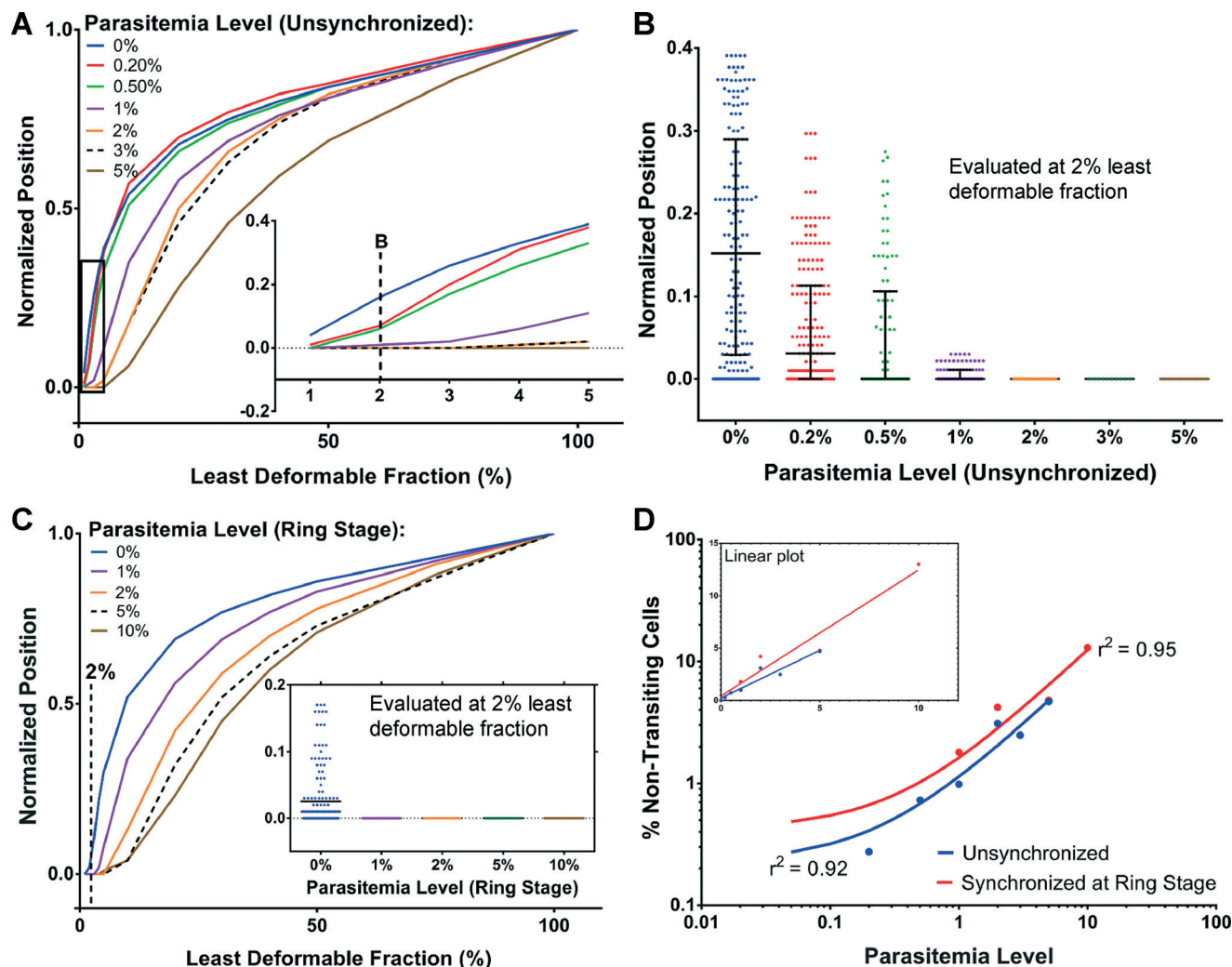


Fig. 4 Deformability-based detection of malaria. (A) The deformability profiles of RBCs parasitized with unsynchronized *P. falciparum* at increasing population fraction from least to most deformable ($n = 8575$ for control and an $n \geq 500$ for 3% parasitemia level). (B) Detailed deformability profile of (A) at 2% least deformable fraction shows significant difference between 0% and 0.2% parasitemia samples ($p < 0.0001$). (C) Deformability profiles of RBCs parasitized with ring-synchronized *P. falciparum* at increasing population fraction from least to most deformable. The detailed deformability profile evaluated at 2% least deformable population (insert) shows a significance difference between 0% and 1% parasitemia samples ($p < 0.0001$, $n = 9074$ for control and an $n \geq 978$ for 2% parasitemia level). (D) A strong, positive correlation between parasitemia level and percentage of non-transiting cells is plotted at log-log scale ($r^2 \geq 0.92$) and (insert) at linear scale.

derivatives rigidify iRBCs and increases splenic retention of these cells.⁴⁹ The mechanism for chloroquine-mediated rigidification of iRBCs is by drug-induced inhibition of hemozoin biocrystallization,⁵⁴ which contributes to intracellular free heme that induces oxidative damage and rigidification of the cell membrane.⁴⁸ In contrast to chloroquine, the mechanism-of-action for artemisinin is not well established but is thought to stimulate reactive oxygen species (ROS) to crosslink cytoskeletal thiols and rigidify the cell.⁵⁵ Currently, it is not known whether this phenomenon extends broadly to all antimalarials or whether it has a functional role in malaria pathogenesis. To investigate this issue, we screened all 9 clinical antimalarials by treating purified iRBCs at $4 \times EC_{50}$ concentrations for 4 hours.

We found significant loss of iRBC deformability following exposure to antimalarials is a nearly universal phenomenon

(Fig. 5A and B, $p < 0.0001$), with an average 44% difference in the normalized transiting distance from control (ESI S9†). As negative control, we also measured the deformability of uninfected RBCs after exposure to the same antimalarial drugs and found no significant effect (ESI S8†). The lone exception to the observed phenomenon of reduced iRBC deformability after exposure to clinical antimalarials was tetracycline ($p = 0.54$), a protein synthesis inhibitor that is slow acting and requires more than 48 hours of incubation to be effective.⁵⁶ It is therefore unlikely that tetracycline could exert a significant change in iRBC deformability during the 4 hour incubation time. This result suggests that rigidification of iRBCs is a universal property of all antimalarials. Given the established relationship between cell rigidification and iRBC splenic clearance,⁴⁹ specific changes in iRBC deformability may represent a common mode of action for these drugs,

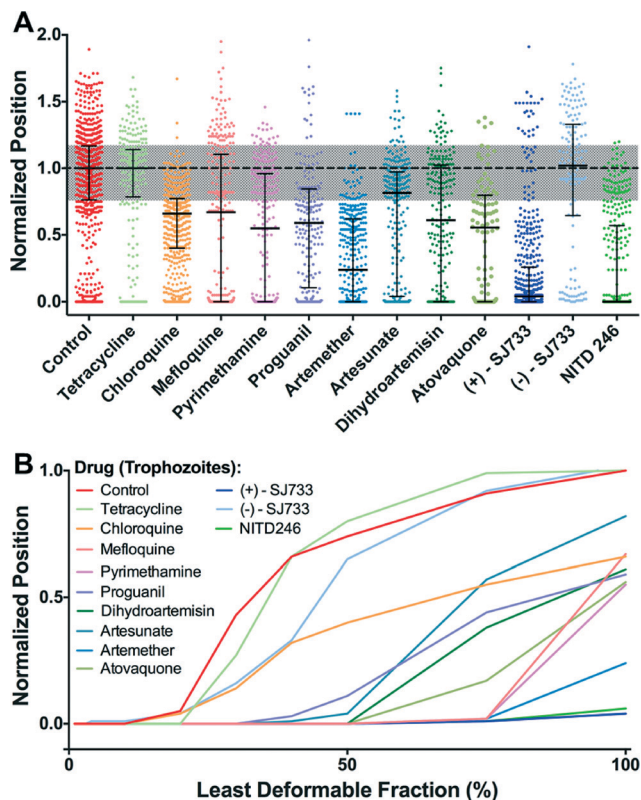


Fig. 5 The evaluation of the efficacy of antimalarial drugs. (A) Scatter-plots of the antimalarial drug response ($\geq 4 \times EC_{50}$) in late-stage RBCs infected with *P. falciparum* parasites show decreased deformability for all antimalarial drugs ($p < 0.0001$) except tetracycline ($p = 0.54$) and (-)-SJ733, which is inactive vs. malaria ($p = 0.1$) with $n \geq 100$ for all samples. (B) Cumulative distribution curves of the least deformable late-stage iRBCs treated with antimalarial drugs.

making it a highly relevant biomarker for use in functional screens of prospective antimalarial compounds.

We further studied the effect on iRBC deformability after exposure to two recently discovered antimalarials from the spiroindolone family, (+)-SJ733 and NITD-246, which inhibit the *Pf*ATP4 cation-transporting ATPase that maintain low intracellular Na^+ levels in the parasite. Disruption of this transporter promotes Na^+ extrusion and reduced iRBC pH.⁵⁷ Intra-erythrocyte acidification accelerates host cell senescence⁵⁸ and reduces host cell deformability.⁵⁹ These spiroindolones were noted to promote rapid host-mediated clearance of iRBCs that was consistent with significant rigidification of the host cells.⁵⁸ Interestingly, our survey of antimalarial compounds showed that these compounds induced the greatest rigidification of iRBCs (Fig. 5A and B). Importantly, tests on the inactive (-)-SJ733 enantiomer⁵⁸ resulted in no change in iRBC deformability ($p = 0.1$), which confirms the loss of deformability is a specific antimalarial effect.

Discussion

Microfluidic cell-phoresis provides a simple, sensitive, and multiplexed biophysical assay for RBC deformability. The

importance of RBC deformability in a range of hematological diseases has been widely accepted but measurement of RBC deformability is difficult. RBC deformability is typically inferred from either the bulk rheological properties of blood^{11–16} or from a direct measurement of a small number of cells.^{17–24} In contrast, microfluidic cell-phoresis enables rapid measurement of the deformability of a statistically relevant number of individual cells. The method is also highly sensitive, discriminating between normal RBCs and those treated with 0.0005% GTA. The combination of high sample throughput and measurement sensitivity makes this system ideal for integration into a drug discovery platform.

Examination of the biophysical signature of RBCs parasitized by falciparum malaria represents an effective model to evaluate the potential for this system in drug discovery. In falciparum malaria, parasitized cells exhibit a subtle decrease in cell deformability at ring stage that progresses to a significant rigidification of the host cell by the mature schizont stage.³¹ Using the microfluidic cell-phoresis mechanism, we demonstrated calibration-free detection of infection in both unsynchronized and ring-stage synchronized cultures. We further observed that reduced deformability specific to iRBCs was a common feature among clinical antimalarials, suggesting that iRBC deformability may be a universal biomarker for antimalarial drug efficacy. Change in iRBC deformability is a particularly compelling biomarker for antimalarial drug efficacy because of its potential contribution to host-mediated parasite clearance,⁴⁹ as well as the proposed mechanisms by which chloroquine and artemisinins may contribute to host cell rigidification.^{48,55} Further support for the central role of drug-induced iRBC rigidification in parasite clearance comes from emerging *Pf*ATP4 inhibitors, (+)-SJ733 and NITD-246, which have been reported to induce rapid host-mediated parasite clearance.⁵⁸ These compounds displayed significantly greater reduction in host cell deformability compared to traditional antimalarials and showed a distinct signature in their deformability profile. These results suggest the potential to use microfluidic cell-phoresis to screen for new antimalarial compounds, as well as to elucidate their mechanisms of action.

Existing assays for antimalarial efficacy are mainly based on survival of parasites grown in culture, but provide little information on the mechanism of action of the drug or its potential for *in vivo* clearance. Consequently, compounds that show less activity, but are otherwise biologically tractable may be excluded at an early stage from the screening process. While the relationship between iRBC deformability and clinical outcomes in falciparum malaria is currently unclear, the availability of simple experimental tools would enable these studies. By elucidating the specific cellular response that corresponds to successful clearance of the parasite, it may be possible to screen agents that act as adjunctive therapies to use in combination with traditional antimalarials in order to reduce toxicity and drug-resistance. It is even possible to envision scenarios where RBC deformability assays could be used during treatment to test patient iRBCs against multiple

therapies in order to select the most effective course of treatment. It may even be possible to extract separated RBCs for further analysis, however, significant challenges exist due to the small number of RBCs in this sample.

Finally, while malaria was the model selected for this study, RBC deformability is affected within a wide spectrum of hematological disorders. In many cases, the change in RBC deformability may only be detectable in a small proportion of the cell population. For this reason, detection of these poorly deformable RBCs based on the rheological properties of blood or the measured deformability of single cells may fail to detect these changes. Sensitive and high-throughput measurement of single RBCs allows for subtle changes in RBC deformability to provide valuable insight into many of these disorders and may provide a sensitive indicator of general health.

Material and methods

Device fabrication

Master wafers for the microfluidic cell-phoresis devices were fabricated on silicon wafer substrates using photolithography of three different types of SU8 photoresist. SU-8 3005, SU-8 2015 and SU-8 3025 (MicroChem, Newton, MA, USA) were used to fabricate the deformation microchannels, the alignment marks and the remaining microstructures respectively. The patterns for the microstructures were drawn using DraftSight. The thicknesses of the microstructures were measured using a profilometer (Alpha Step 200) and the porosities were measured using fluorescence microscopy.

Microfluidic devices were made using soft lithography of polydimethylsiloxane (PDMS) silicon. To minimize degradation of the master silicon wafer, polyurethane-based (Smooth-Cast ONYX, Smooth-On) molds were fabricated as a replica of the master wafers *via* a process described by Desai *et al.*⁶⁰ Microfluidic device was made by mixing Sylgard-184 PDMS (Ellsworth Adhesives) base at a ratio of 10:1 (w/w) to its hardener, after which the mixture was poured into the replica mold and degassed for 15 minutes. The device was then baked for 2 hours at 65 °C and reservoir holes were punched on the device using a 4 mm hole punch (Technical Innovations, Angleton, TX, USA). A thin layer of RTV615 PDMS (10:1 ratio of base to hardener) was spin-coated onto a blank wafer and baked for 1 hour at 65 °C. The microfluidic device and the PDMS coated wafer were bonded together after oxidizing them separately in oxygen plasma chamber (Harrick Plasma, Ithaca, NY) for 80 s. For the final step, the resulting device was bonded to a 50 × 75 mm glass slide (Fisher Scientific).

Experimental set-up

Instrumentation for the cell transport dispersion device consists of an optical imaging system and a pneumatic pressure control system. The former includes an inverted microscope to observe the microfluidic device using a 4× objective and a high-resolution camera. A bandpass filter (Edmund Optics, US)

was used to produce sharper image contrast between RBCs and the microchannels for easier detection by the image processing software. The filter only passes light with a wavelength of 420 nm, which is absorbed by RBCs, making RBCs appear black and hence, distinct from debris and bubbles. The camera system (17 fps) acquires images to observe the cell loading process and capture the final position of the cells after transporting them in the deformation microchannel. A low microscope magnification and a high camera resolution are desirable to detect as many cells as possible in each camera frame. The pneumatic pressure control system applies a variable pressure to the sample and buffer reservoirs in order to first load the sample cells and then transport them through the deformation microchannels. The variable pressure will be generated using a Fluigent (Paris, France) pressure control system and controlled from a PC.

Image processing software was developed in-house using C# to measure the final position of the cells after applied deformation pressure. This software is semi-automatic and allowed users to set reference positions within the device, after which it would automatically recognize the cells and determine the cell position in the deformation microchannel. The cell position within the deformation microchannel is determined by the center position of the cells (ESI S3†). For higher measurement accuracy, the software also gave users the ability to manually select the cells that the software might miss. A potential source of error occurs when multiple cells enter one deformation microchannel. The image processing software removed these cells from the measurement.

Cell sample preparation

Device validation was performed using normal fresh whole blood obtained from consenting donors by finger-prick (Unistik 3, Owen Mumford, Fisher) or venipuncture. Blood was diluted with Phosphate Buffered Saline (PBS, Gibco) into 20% hematocrit and 0.2% Pluronic F127 (Sigma) solution was added to it.

Device sensitivity experiments were performed using whole blood that was chemically treated to reduce deformability by mild fixation using glutaraldehyde (GTA). GTA is known to rigidify RBCs by cross-linking proteins in the cell membrane. By increasing the GTA concentration, a sample with a known trend in deformability profile is obtained. GTA was added to RBCs at 5% hematocrit at a concentration between 0.0005–0.002% and incubated at room temperature for 30 minutes. After the incubation period, the sample was washed 3 times with PBS and finally, the GTA-treated blood samples were diluted to 20% hematocrit in PBS with 0.2% Pluronic added to it.

RBCs infected with *P. falciparum* (3D7 strain) will be prepared using standard *in vitro* culture methods, and in some cases, synchronized to obtain infected RBCs at specific stages of parasite growth as described by Radfar, *et al.*⁶¹ Donor RBCs with A+ and O+ blood type were obtained with informed consent from Canadian Blood Services and were

infected with *P. falciparum*. The culture was incubated in a hypoxic chamber (3% O₂ and 5% CO₂) at 37 °C and was maintained in RPMI-1640 culture media (Invitrogen) containing 25 mM HEPES (Sigma), 0.5% (wt/vol) AlbuMAX I (Life Technologies), 100 μM hypoxanthine (Sigma), 12.5 μg ml⁻¹ gentamicin (Sigma) and 1.77 mM sodium bicarbonate (Sigma). Before each experiment, parasitemia level was measured using Giemsa staining (Sigma-Aldrich),⁶¹ in which Giemsa stain was diluted at a 1:2 volume ratio with PBS (ESI†). Infected RBCs (iRBCs) were then diluted using uninfected blood to the desired parasitemia level. The uninfected RBCs followed the same incubation period as the iRBC sample and was used as the control for every experiment involving malaria detection.

Purified iRBCs were obtained by passing the culture sample through a LS column (Miltenyl Biotec) surrounded by Neodymium Super Magnets (Applied Magnets).⁶² Since iron-containing hemozoin was present in late-stage iRBCs, they were held in the magnetic column and could be extracted from the column using a syringe. The purified iRBCs were resuspended in RPMI medium and incubated for 30 minutes in the hypoxic chamber, after which the parasites were treated with various anti-malarial drugs at different concentrations for 4 hours. Known drugs were tested at concentrations >EC50 of each drug: 1 μM chloroquine, 1 μM, 20 nM pyrimethamine, 100 μM proguanil, 10 nM artesunate, 8 nM artemether, 20 nM dihydroartemisinin, 100 μM tetracyclines, 250 nM atovaquone, 1.08 μM for both enantiomers of dihydroisoquinolone – SJ733 and 3.6 nM for spiroindolone NITD 246.^{56,58,63,64} Since drugs were diluted in DMSO, untreated iRBCs were treated with 0.01% DMSO and acted as the control.

Synchronized sample at the ring-stage was produced by sorbitol lysis⁶¹ and was diluted using uninfected blood to the desired parasitemia level. A highly synchronized culture of rings with ~10% parasitemia was treated with chloroquine, artesunate, NITD and DHIQ anti-malarial drug with the same concentrations used for the purified iRBCs.

References

- 1 S. Magdeldin, Y. Zhang and B. Xu, *Gel Electrophoresis - Principles and Basics*, InTech, 2012.
- 2 G. Y. H. Lee and C. T. Lim, *Trends Biotechnol.*, 2007, 25, 111–118.
- 3 G. B. Nash, E. O'Brien, E. C. Gordon-Smith and J. A. Dormandy, *Blood*, 1989, 74, 855–861.
- 4 T. Herricks, M. Antia and P. K. Rathod, *Cell. Microbiol.*, 2009, 11, 1340–1353.
- 5 L. H. Miller, D. I. Baruch, K. Marsh and O. K. Doumbo, *Nature*, 2002, 415, 673–679.
- 6 M. D. Scott, P. Rouyer-Fessard, M. S. Ba, B. H. Lubin and Y. Beuzard, *Br. J. Haematol.*, 1992, 80, 519–526.
- 7 G. A. Barabino, M. O. Platt and D. K. Kaul, *Annu. Rev. Biomed. Eng.*, 2010, 12, 345–367.
- 8 A. Vayá, M. Simó, M. Santaolara, J. Todolí and J. Aznar, *Clin. Hemorheol. Microcirc.*, 2005, 33, 75–80.
- 9 R. Yip, N. Mohandas, M. R. Clark, S. Jain, S. B. Shohet and P. R. Dallman, *Blood*, 1983, 62, 99–106.
- 10 W. H. Reinhart, *Br. J. Haematol.*, 1992, 80, 550–555.
- 11 M. Bessis, N. Mohandas and C. Feo, *Blood Cells*, 1980, 6, 315–327.
- 12 M. R. Clark, N. Mohandas and S. B. Shohet, *Blood*, 1983, 61, 899–910.
- 13 O. K. Baskurt, M. R. Hardeman, M. Uyklu, P. Ulker, M. Cengiz, N. Nemeth, S. Shin, T. Alexy and H. J. Meiselman, *Biorheology*, 2009, 46, 251–264.
- 14 G. J. Streekstra, J. G. G. Dobbe and A. G. Hoekstra, *Opt. Express*, 2010, 18, 14173–14182.
- 15 T. L. Berezina, S. B. Zaets, C. Morgan, C. R. Spillert, M. Kamiyama, Z. Spolarics, E. A. Deitch and G. W. Machiedo, *J. Surg. Res.*, 2002, 102, 6–12.
- 16 R. L. Newman, *J. Clin. Pathol.*, 1964, 17, 194–195.
- 17 R. P. Hebbel, A. Leung and N. Mohandas, *Blood*, 1990, 76, 1015–1020.
- 18 E. A. Evans, R. Waugh and L. Melnik, *Biophys. J.*, 1976, 16, 585–595.
- 19 E. Evans, N. Mohandas and A. Leung, *J. Clin. Invest.*, 1984, 73, 477–488.
- 20 I. Dulińska, M. Targosz, W. Strojny, M. Lekka, P. Czuba, W. Balwierz and M. Szymoński, *J. Biochem. Biophys. Methods*, 2006, 66, 1–11.
- 21 M. Lekka, M. Fornal, G. Pyka-Fościk, K. Lebed, B. Wizner, T. Grodzicki and J. Styczeń, *Biorheology*, 2005, 42, 307–317.
- 22 J. P. Mills, L. Qie, M. Dao, C. T. Lim and S. Suresh, *Mech. Chem. Biosyst.*, 2004, 1, 169–180.
- 23 S. Hénon, G. Lenormand, A. Richert and F. Gallet, *Biophys. J.*, 1999, 76, 1145–1151.
- 24 M. Dao, C. T. Lim and S. Suresh, *J. Mech. Phys. Solids*, 2003, 51, 2259–2280.
- 25 J. P. Shelby, J. White, K. Ganesan, P. K. Rathod and D. T. Chiu, *Proc. Natl. Acad. Sci. U. S. A.*, 2003, 100, 14618–14622.
- 26 G. Tomaiuolo, M. Barra, V. Preziosi, A. Cassinese, B. Rotoli and S. Guido, *Lab Chip*, 2011, 11, 449–454.
- 27 A. Adamo, A. Sharei, L. Adamo, B. Lee, S. Mao and K. F. Jensen, *Anal. Chem.*, 2012, 84, 6438–6443.
- 28 H. Bow, I. V. Pivkin, M. Diez-Silva, S. J. Goldfless, M. Dao, J. C. Niles, S. Suresh and J. Han, *Lab Chip*, 2011, 11, 1065–1073.
- 29 Y. Zheng and Y. Sun, *Micro Nano Lett.*, 2011, 6, 327.
- 30 Q. Guo, S. M. McFaul and H. Ma, *Phys. Rev. E: Stat., Nonlinear, Soft Matter Phys.*, 2011, 83, 051910.
- 31 Q. Guo, S. J. Reiling, P. Rohrbach and H. Ma, *Lab Chip*, 2012, 12, 1143–1150.
- 32 M.-E. Myrand-Lapierre, X. Deng, R. R. Ang, K. Matthews, A. T. Santoso and H. Ma, *Lab Chip*, 2015, 15, 159–167.
- 33 D. Holmes, G. Whyte, J. Bailey, N. Vergara-Irigaray, A. Ekpenyong, J. Guck and T. Duke, *Interface Focus*, 2014, 4, 20140011.
- 34 Q. Guo, S. P. Duffy, K. Matthews, X. Deng, A. T. Santoso, E. Islamzada and H. Ma, submitted.

- 35 Q. Guo, S. P. Duffy, K. Matthews, A. T. Santoso, M. D. Scott and H. Ma, *J. Biomech.*, 2014, **47**, 1767–1776.
- 36 M. Komorowska, M. Koter, G. Bartosz and J. Gomulkiwicz, *Biochim. Biophys. Acta*, 1982, **686**, 94–98.
- 37 T. L. Steck, *J. Mol. Biol.*, 1972, **66**, 295–305.
- 38 X. Liu, Z. Tang, Z. Zeng, X. Chen, W. Yao, Z. Yan, Y. Shi, H. Shan, D. Sun, D. He and Z. Wen, *Math. Biosci.*, 2007, **209**, 190–204.
- 39 A. M. Forsyth, J. Wan, W. D. Ristenpart and H. A. Stone, *Microvasc. Res.*, 2010, **80**, 37–43.
- 40 G. Tomaiuolo and S. Guido, *Microvasc. Res.*, 2011, **82**, 35–41.
- 41 G. Tomaiuolo, *Biomicrofluidics*, 2014, **8**, 051501.
- 42 N. Mohandas and X. An, *Med. Microbiol. Immunol.*, 2012, **201**, 596–598.
- 43 J. P. Mills, M. Diez-Silva, D. J. Quinn, M. Dao, M. J. Lang, K. S. W. Tan, C. T. Lim, G. Milon, P. H. David, O. Mercereau-Puijalon, S. Bonnefoy and S. Suresh, *Proc. Natl. Acad. Sci. U. S. A.*, 2007, **104**, 9213–9217.
- 44 K. L. Waller, W. Nunomura, X. L. An, B. M. Cooke, N. Mohandas and R. L. Coppel, *Blood*, 2003, **102**, 1911–1914.
- 45 N. Mohandas, X. H. Pei, X. L. An, X. H. Guo, M. Tarnawski and R. Coppel, *J. Biol. Chem.*, 2005, **280**, 31166–31171.
- 46 D. I. Baruch, B. L. Pasloske, H. B. Singh, X. Bi, X. C. Ma, M. Feldman, T. F. Taraschi and R. J. Howard, *Cell*, 1995, **82**, 77–87.
- 47 B. M. Cooke, N. Mohandas and R. L. Coppel, *Adv. Parasitol.*, 2001, **50**, 1–86.
- 48 F. Nuchsongsin, K. Chotivanich, P. Charunwatthana, O. S. Fausta, D. Taramelli, N. P. Day, N. J. White and A. M. Dondorp, *Am. J. Trop. Med. Hyg.*, 2007, **77**, 617–622.
- 49 S. Huang, A. Amaladoss, M. Liu, H. Chen, R. Zhang, P. R. Preiser, M. Dao and J. Han, *Infect. Immun.*, 2014, **82**, 2532–2541.
- 50 A. M. Dondorp, E. Pongponratn and N. J. White, *Acta Trop.*, 2004, **89**, 309–317.
- 51 A. M. Dondorp, C. Ince, P. Charunwatthana, J. Hanson, A. van Kuijen, M. A. Faiz, M. R. Rahman, M. Hasan, E. Bin Yunus, A. Ghose, R. Ruangveerayut, D. Limmathurotsakul, K. Mathura, N. J. White and N. P. J. Day, *J. Infect. Dis.*, 2008, **197**, 79–84.
- 52 R. Dayal, C. Decrind and P. H. Lambert, *Bull. W. H. O.*, 1986, **64**, 403–414.
- 53 A. M. Dondorp, P. A. Kager, J. Vreeken and N. J. White, *Parasitol. Today*, 2000, **16**, 228–232.
- 54 A. F. G. Slater and A. Cerami, *Nature*, 1992, **355**, 167–169.
- 55 S. R. Meshnick, Y. Z. Yang, V. Lima, F. Kuypers, S. Kamchonwongpaisan and Y. Yuthavong, *Antimicrob. Agents Chemother.*, 1993, **37**, 1108–1114.
- 56 E. L. Dahl and P. J. Rosenthal, *Antimicrob. Agents Chemother.*, 2007, **51**, 3485–3490.
- 57 N. J. Spillman, R. J. W. Allen and K. Kirk, *Mol. Biochem. Parasitol.*, 2013, **189**, 1–4.
- 58 M. B. Jiménez-Díaz, D. Ebert, Y. Salinas, A. Pradhan, A. M. Lehane, M.-E. Myrand-Lapierre, K. G. O’Loughlin, D. M. Shackleford, M. Justino de Almeida, A. K. Carrillo, J. A. Clark, A. S. M. Dennis, J. Diep, X. Deng, S. Duffy, A. N. Endsley, G. Fedewa, W. A. Guiguemde, M. G. Gómez, G. Holbrook, J. Horst, C. C. Kim, J. Liu, M. C. S. Lee, A. Matheny, M. S. Martínez, G. Miller, A. Rodríguez-Alejandre, L. Sanz, M. Sigal, N. J. Spillman, P. D. Stein, Z. Wang, F. Zhu, D. Waterson, S. Knapp, A. Shelat, V. M. Avery, D. A. Fidock, F.-J. Gamo, S. A. Charman, J. C. Mirsalis, H. Ma, S. Ferrer, K. Kirk, I. Angulo-Barturen, D. E. Kyle, J. L. DeRisi, D. M. Floyd and R. K. Guy, (+)-SJ733, a clinical candidate for malaria that acts through ATP4 to induce rapid host-mediated clearance of Plasmodium, *Proc. Natl. Acad. Sci.*, 2014, **111**, E5455–E5462.
- 59 D. Kuzman, T. Znidarcic, M. Gros, S. Vrhovec, S. Svetina and B. Zeks, *Pflugers Arch.*, 2000, **440**, R193–R194.
- 60 S. P. Desai, D. M. Freeman and J. Voldman, *Lab Chip*, 2009, **9**, 1631–1637.
- 61 A. Radfar, D. Méndez, C. Moneriz, M. Linares, P. Marín-García, A. Puyet, A. Diez and J. M. Bautista, *Nat. Protoc.*, 2009, **4**, 1899–1915.
- 62 S. Hackett, J. Hamzah, T. M. E. Davis and T. G. Pierre St., *Biochim. Biophys. Acta*, 2009, **1792**, 93–99.
- 63 J. Mu, R. A. Myers, H. Jiang, S. Liu, S. Ricklefs, M. Waisberg, K. Chotivanich, P. Wilairatana, S. Krudsood, N. J. White, R. Udomsangpetch, L. Cui, M. Ho, F. Ou, H. Li, J. Song, G. Li, X. Wang, S. Seila, S. Sokunthea, D. Socheat, D. E. Sturdevant, S. F. Porcella, R. M. Fairhurst, T. E. Wellems, P. Awadalla and X. Su, *Nat. Genet.*, 2010, **42**, 268–271.
- 64 L. Vivas, L. Rattray, L. B. Stewart, B. L. Robinson, B. Fugmann, R. K. Haynes, W. Peters and S. L. Croft, *J. Antimicrob. Chemother.*, 2007, **59**, 658–665.